Photo-Electrochemical Investigation of Inorganic/Organic Interfaces Assembly Consisting of Zn-Doped WO_3 /Poly 4-(Thiophen-3-yl) Aniline.

Kasem K. Kasem, Heather Ramey & Christopher Santucci

[1]School of Sciences, Indiana University Kokomo, Kokomo, IN, 46904, USA

Correspondence: Kasem K. Kasem, School of Sciences, Indiana University Kokomo, Kokomo, IN, 46904, USA. E-mail: kkasem@iuk.edu

Abstract

Photoactivities at inorganic/Organic/Interfaces (IOI) consisting of Zn-doped WO_3 (Zn-WO_3) /Poly 4-(Thiophen-3-yl) aniline (P3ThA) assemblies were investigated in nanoparticle suspensions and in thin solid film forms. The effects of P3ThA modifier on the photoelectrochemical behavior of the IOI were investigated using $[Fe(CN)_6]^{4-}$ as a photoactive donor of hydrated electrons. Results show that the adsorption process of $[Fe(CN)_6]^{3-}$ (photolysis product) controls the photoactivity outcomes of the IOI assemblies. P3ThA shows a greater heterogeneous photochemical response than native Zn-WO_3. The band alignment between Zn-WO_3 and P3ThA is of a p-p junction straddling gap type, where the charge transfer process is achieved through a hole transfer mechanism. The interface activities were explained by analyzing the IOI junction characteristics such as electron affinity, work function and hole/electron barrier heights. The creation of hybrid sub-band states close to the Fermi energy level at the interface was suggested. The aqueous nano-systems retained moderate stability as indicated by the reproducibility of their photocatalytic activities. Both $[Fe(CN)_6]^{4-}$ and P3ThA contributed to the stability of the native Zn-WO_3 surfaces.

Keywords: photoelectrochemistry, semiconductors, solar energy, heterojunctions

1. Introduction

The quest for improving the solar to electrical energy conversion efficiencies in photovoltaic assemblies involved many techniques including the creation of the hybrid Inorganic/Organic interfaces or [IOI] (Wang Y. et al 2011, Kasem K. et al, 2008, Thomas K.G. et al 2003). The hetero-junction at the IOI assembly can affect its chemical, electrochemical, optical, magnetic and mechanical properties. Creating effective IOI requires energy coordination between the organic and inorganic interfaces for efficient charge transfer and separation as in heterojunction-type assemblies. Information about physical quantities such as electronegativity [𝜘], Electron affinity [EA] , work function [Φ], barrier height [φ] and band gap [E_g] for components of the IOI will help understanding how the heterojunction assemblies work.

Surface modification caused by formation of IOIs, can be a very effective way to create or eliminate defects and alter the energy band at inorganic /organic interfaces. This will also alter the donor /acceptor character of the IOI assemblies. Recent studies show that binary oxides can provide more efficient charge separation, increased lifetime of charge carriers and enhanced interfacial charge transfer to absorbed substrates (Wang C. et al, 2002, Liao D.L. et al, 2008, Wang Y. et al, 2011, Kasem K. et al, 2008, Thomas K.G. et al, 2003, Kasem K. et al, 2009, Zhang, Qichun et al, 2008). Some metal chalcogenides modified with poly-aniline, poly-pyrrole, or other organic semiconductors were studied (Wang Y. et al, 2011, Kasem K. et al, 2008, Thomas K.G. et al, 2003, Kasem K. et al, 2009, Zhang, Qichun et al, 2008). Special assemblies of narrow band gap semiconductor nanostructures can be convenient systems for capturing visible light energy. Metal/ chalcogenides/ oxide semiconductors absorb only solar radiation that matches their band gaps. However, the spectral range can be widened if the metal sulfides surfaces are modified with agent/s that can absorb or become excited by greater radiation energies, such as UV. Some conjugated organic semiconductors absorb UV radiation and then re-emit radiation at longer wavelengths.

Several studies have been carried out in searching for organic semiconductors that can act as a modifier in IOI assemblies. Copolymers consisting of 2,1,3-benzoselenadiazole and carbazole derivatives with thiophene were found to generate low-band gap materials (Kim, Ji-Hoon et al, 2014). Opto-electrochemical properties of selenopheno [3,2-c]thiophene as a low band gap conjugated polymer has been investigated (Jo, Yu-Ra et al,

2011). Furthermore, electrochemical copolymerizations of thiophene derivatives were used in building photovoltaic devices (Kumar, Prajwal et al, 2011), or Ion selective sensors (Pengchao Si, et al 2007) . Synthesis, thermal and optoelectrochemical properties of symmetrical conjugated thiophene and tri-phenylamine have been investigated (Vacareanu, Loredana et al, 2012). A study (Bondock, Samir et al, 2010) shows that the title compound is related to category of compounds that has a proven antimicrobial activity.

The compound 4-[thiophen-3-yl] aniline [3ThA] consists of thiophene and aniline that can be polymerized by chemical, photo-, and electro-chemical methods. The proposed structure of P3ThA is illustrated in Figure 1 inset C. Both polymer based aniline and polymer based thiophene have moderate to low band gap characters. No previous studies are made on the photoelectrochemical behavior of 3ThA. In the present work we report some of the photoelectrochemical behavior of 3ThA as the organic part of IOI assembly consists of Zn-doped WO_3 /P3ThA nanoparticles. Furthermore, the effectiveness of this assembly in hydrogen production during the photolysis of aqueous suspensions of nanoparticles of this assembly containing $[Fe[CN]_6]^{4-}$ is explored. Results correlate of the information about electronegativity [EA], Electron affinity [$\varkappa$] , work function [Φ], barrier height [φ] band gap [Eg] and energy band alignments for components of the IOI .

2. Experimental

2.1 Reagents

All the reagents were of analytical grade. All of the solutions were prepared using deionized water, unless otherwise stated. Zn-WO_3 / P3ThA were either in nanoparticles form or thin solid films.

2.2 Preparations

P3ThA: This polymer was prepared by both electrochemical and photochemical techniques:

A-   Electropolymerization of P3ThA.

Polymer thin films were generated electrochemically using cyclic voltammetry (CV) by repetitive cycling of the FTO electrode potential at a scan rate 0.10V/s between -1.0 and 2.0 V vs Ag/AgCl in acetonitrile of 1 mM of 3ThA and 0.5M $LiClO_4$.

B- (Occlusion Method): Thin films of Zn-WO_3 / (P3ThA) were generated electrochemically using cyclic voltammetry (CV) by repetitive cycling of the FTO electrode between -1.0 and 2.0 V vs Ag/AgCl in acetonitrile suspension of Zn-WO_3, 1 mM of the monomer and 0.5M $LiClO_4$.

C- Preparation of Zn-Doped WO_3 / P3ThA / Interface:

Colloidal suspensions of Zn-doped WO_3 / P3ThA interface were prepared as follows: 0.05 g of Zn-doped WO_3 nanoparticles prepared as reported previously (Kalyanasundaram K. et al 1998) were suspended in the solution of 3-ThA in acetonitrile. The mixture was subjected to a 10 minute sonication followed by stirring for 1.0 hour to allow maximum adsorption of P3ThA on the Zn-doped WO_3 nanoparticles. The excess P3ThA was removed by centrifugation. Zn-doped WO_3 with adsorbed P3ThA was re-suspended in deionized water containing few drops of H_2O_2 and subjected to UV radiation under constant stirring for 3 hours. The resultant Zn-Doped WO_3 / P3ThA was rinsed with deionized water several times and allowed to dry at 120 °C for 2 hours.

D-   Deposition of Zn-Doped WO_3 / P3ThA Thin Solid Films:

Thin solid films of Zn-Doped WO_3 particles, modified with P3ThA (prepared as described in C) were suspended in acetonitrile solution of poly vinyl pyridine (PVP). The suspension was evenly spread over fluorine doped Tin Oxide (FTO) slides (12.5 x75 mm) and dried at 120 °C for 2 hours. The assembled electrode was transferred to a three-electrode cell containing the chosen buffer as the electrolyte and a Ag/AgCl and Pt electrode as reference and counter electrode, respectively.

2.3 Instrumentation

All electrochemical experiments were carried out using a conventional three-electrode cell consisting of a Pt wire as a counter electrode, Ag/AgCl as a reference electrode, and Pt gauze as an electron collector. A BAS 100W electrochemical analyzer (Bioanalytical Co.) was used to perform the electrochemical studies. Steady state reflectance spectra were performed using Shimadzu UV-2101 PC. Irradiation was performed with a solar simulator 300-watt xenon lamp (Newport) with an IR filter. Photoelectrochemical studies on thin solid films were performed on an experimental set as illustrated in Diagram 1A.

Diagram 1A
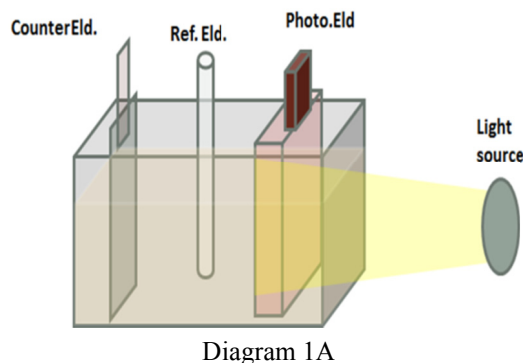
2.4 Photolysis Cell

The illustration of the electrolysis cell was a one-compartment Pyrex cell with a quartz window facing the irradiation source is displayed in previous work (Kasem K. et al 2014) . The working electrode, a 10.0 cm^2 platinum gauze cylinder, had a solution volume of 100 mL. Suspensions were stirred with a magnetic stirrer during the measurements. A Ag/AgCl/Cl- reference electrode was also fitted into this compartment. A 10-cm^2 platinum counter electrode was housed in a glass cylinder sealed in one end with a fine porosity glass frit. Photolysis of $[Fe(CN)_6]^{4-}$ generated hydrated electrons and $[Fe(CN)_6]^{3-}$. The potential of the working electrode was fixed at 100 mV more negative than the reduction potential of $[Fe(CN)_6]^{3-}$ to guarantee full reduction of ferricyanide. The current due to the reduction of $[Fe(CN)_6]^{3-}$ collected by the working electrode during the photolysis process is a measure of photocurrent. The measured photocurrent was normalized considering two photons per one hydrogen molecule, and was used to calculate the number of moles of hydrogen generated per square meter per hour of illumination. Unless otherwise stated, all experiments were performed at room temperature 25 ± 1 ^{o}C.

3. Results and Discussion

3.1 Electropolymerization of 3ThA

Polymer film of P3ThA on FTO was prepared by repetitive cycling of the FTO electrode potential at scan rate of 0.10V/s between -1.2 and 2.0 V *vs* Ag/AgCl in acetonitrile solution containing 5 mM of 3THA monomer and 0.5M LiClO$_4$. The results are displayed in Figure 1. The large anodic peaks at 1.10 and 1.6 V developed in the first scan are indication that an oxidative electropolymerization process took place leading to the formation of a compact film. Such anodic peaks start to get smaller in the scans that follow the first scan. The first anodic peak at (ca 1.1 V vs Ag/AgCl) is due to the polymerization of thiophene portion of the monomer at the 2,2' position , while the anodic peak at more positive potential (ca 1.7 V vs Ag/AgCl) is possible due to polymerization of some entrapped monomers in the polymeric film or oxidation of aniline portion of the polymer. The fact that very robust and adhesive film was observed after the first scan or after several scan roles out any decomposition of the polymer film.
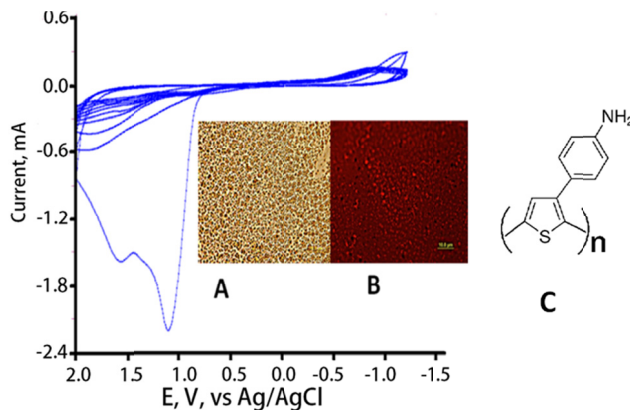
Figure 1. Electropolymerization of 3ThA on ITO. Scan numbers are indicated. Insets A &B are for ITO/ P3ThA/Zn-WO$_3$ assembly created by occlusion electrodeposition of Zn-WO$_3$ with PHA under A) white Light , and B) green (520 nm) Light. Inset C is the proposed structure of PTHA

3.2 Absorption Spectra of P3ThA

Absorption spectra of the monomer 3ThA and the polymer P3ThA over FTO electrode were studied and the results are displayed in Figure 2A and B. Figure 2A indicates that the monomer shows absorbance in a range between 380- 410 nm, while the polymer spectra (Figure 2B[a]) shows a broad or overlapped absorbance peak in the range between 410 to 480 nm. For comparison, the spectra of polymerized 4-[thiophen-2-yl] aniline (2ThA) were also recorded (Figure 2B[b&c]).
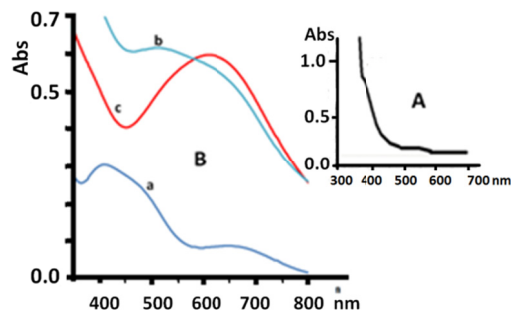
Figure 2. A) Absorption spectra for 4-(Thiophen-3-yl) aniline B) Absorption spectra for FTO/P3ThA a) Poly 4-(Thiophen-3-yl) aniline , b) Poly 4-(Thiophen-2-yl) aniline (at-1.0 V vs Ag/AgCl) , c) Poly 4-(Thiophen-2-yl) aniline (at 1.0 V vs Ag/AgCl)

The poly 4-[thiophen-2-yl] aniline (P2ThA) in its oxidized form (Figure 2Bc) or reduced form Figure 2Bb) shows some electro-chromic behavior. The oxidized form (trace c) absorbs at a longer wavelength than the reduced form (trace b) or that of P3ThA (trace a) . These observations suggest that in 2ThA polymerization involved the aniline portion of the monomer to be the major line of π bond conjugation of the polymer instead of being a function group on the polymer as in P3ThA case. It is well known that absorption bands around 490 nm are attributed to π π* excitation in the poly-thiophene backbone (Gerald Zerza et al 2001) . Absorption peaks at wavelengths shorter than 490 nm are indication of poor conjugation system associated with a shorter polymer chain or formation of oligomers. Figure 2B , clearly indicates that P2ThA (trace 2B b & c) possess better conjugation and longer chain structure than P3ThA(trace 2B.a) . Furthermore, the oxidized form of P2ThA (trace c) has a more conjugated system than the reduced form (trace b). Such behavior can be attributed to the involvement of aniline group in the conjugated system during the polymerization process. This also indicates that the polymerization took place by bridging aniline portion of the polymer because of its ortho- position to S in P3ThA. The location of aniline in position 3 from S, causes polymerization to take place by bridging thiophene molecule and avoiding the aniline portion. This may create less conjugation in this polythiophene derivative than that observed in pure polythiophene. The absorption spectra of P3ThA ranging between 680 to 540 nm are an indication of the energy intervals with high density states that represent higher occupied molecular orbitals (HOMO) and lower unoccupied molecular orbitals (LUMO) of P3THA . This absorption range is corresponding to band gap ranging between 1.8 and 2.3 eV. Such absorption behavior can be attributed to the activity of both the aniline and thiophene rings of the compound. Further analysis that involves calculation of the absorption spectra data of P3ThA (Figure 2B trace a) is displayed in Figure 3. The intercepts in Figure 3 A, show an approximate optical band gap of 2.25 eV, while intercepts in Figure 3B&C are for the indirect and direct band gaps of P3ThA respectively.
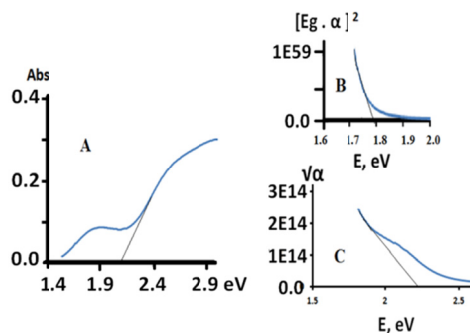
Figure 3. Absorption spectra (A) and Tauc's Plots (B&C) for ITO/P3ThA thin film.

3.2.1 Absorption Spectra of Zn-WO$_3$/ P3ThA IOI Assembly

Absorption spectra of Zn-WO$_3$/ P3ThA thin film over FTO electrode (prepared as described in C in experimental section), were studied and the results are displayed in Figure 4A , B and C. Figure 4A indicates that the IOI assembly shows an absorbance peak at ≈ 450 nm which corresponds to an 2.7 eV band gap. Figures 4 B &C are Tauc's plots derived from Figure 4A. These plots show an indirect and direct band gap transitions at this assembly.
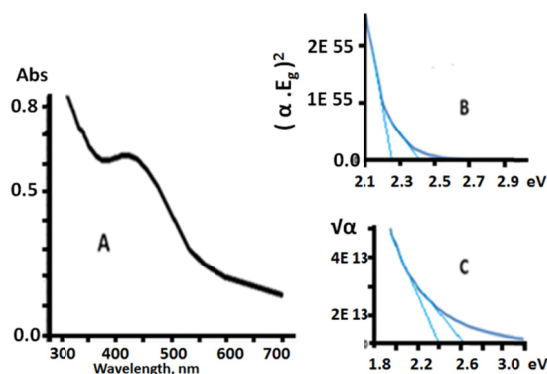
Figure 4. Absorption spectra (A) and Tauc's Plots (B&C) for ITO/P3ThA/Zn-Doped WO$_3$ thin film.

3.2.2 Electrochemical Behavior of P3THA

The electrochemical behavior of P3ThA was investigated by cycling the FTO/ electrode potential at scan rate 0.10V/s between -1.5 to 2.0 V *vs* Ag/AgCl in acetonitrile solution containing 0.5M LiClO$_4$ The results are displayed in Figure 5A. It can be noticed that the onset oxidation potential of this polymer is at ≈ 0.48 V vs Ag/AgCl. Furthermore, Figure 5B illustrates the linear sweep voltammetry for FTO/P3ThA in both NaOH and H$_2$SO$_4$, from which we can observe the effect of the protonation of N in the aniline portion of 3ThA. The protonated polymer has a greater oxidation potential, while un-protonated polymer possesses a lower oxidation potential. It's worth noticing also that under illumination the photocurrent starts to increases at ≈-0.0 vs Ag/AgCl. This value gives the approximate position of the flat band potential (Fermi Level) of P3ThA at 0.2 V vs SHE.
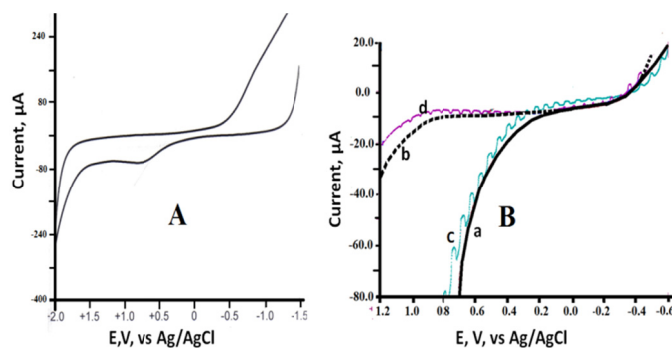
Figure 5. A) CV of FTO/P3ThA in acetonitrile containing 0.5M LiClO$_4$ B: LSV for ITO modified with P3ThA a) NaOH (Dark) b) H$_2$SO$_4$ (Dark)   c) NaOH (Light) d) H$_2$SO$_4$ (Light) Scan rate 0.100 V/s.

3.2.3 Electrochemical Behavior of the Zn-WO$_3$/P3ThA Assembly

Cycling the potential of FTO modified with Zn-WO$_3$/P3ThA assembly at scan rate 0.10V/s , between -1.5 to 2.0 V *vs* Ag/AgCl in acetate buffer pH 8, the results are displayed in Figure 6A. It can be noticed that the current recorded under dark conditions is greater than that recorded under illumination. Figure 6B shows change of photocurrent at -0.5 V under illumination vs dark periods. Figure 6C indicates that illumination generates more of anodic current (notice the chopped trace CV).
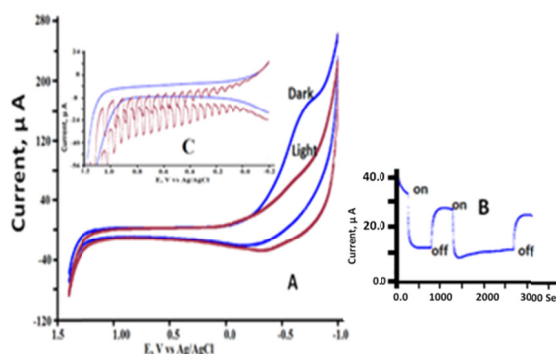
Figure 6. Zn-WO$_3$/ P3ThA in Acetate buffer pH 8. A) CV with 0.1V/s , B) Photocurrent –time base at -0.700 V vs Ag/AgCl C) exploded view for the CV within potential range 0.0 to 1.2 V Vs Ag/AgCl

On the other hand, Figure 7 shows that the behavior of the Zn-WO$_3$/P3ThA assembly is opposite of that displayed in Figure 6. The illumination generates greater cathodic current than that in the dark. The change from phosphate (HPO_4^{2-}) buffer to acetate buffer (CH_3COO^-) clearly alter the nature of donor/acceptor process and consequently alter the mechanism of charge separation and transfer at the IOI electrolyte interface.
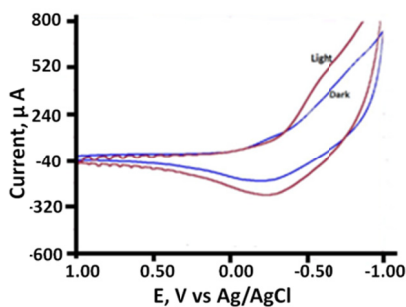
Figure 7. Zn-WO$_3$/ P3ThA in0.2M Phosphate buffer pH 6. At 0.1V/s

Chronocoulometry of Zn-WO$_3$/P3ThA assembly in acetate buffer pH 8, between -0.3 V and -0.7V vs Ag/AgCl took place with 250 ms charge /discharge time, the obtained chronocoulograms are displayed in Figure 8 . Anson plots for these chronocoulograms indicated that upon illumination of this assembly, the capacitive (double layer) charge increased from 4.3 µC to 15.0 µC. Such observations indicate that this created assembly could have potential applications in capacitors and energy storage devices.
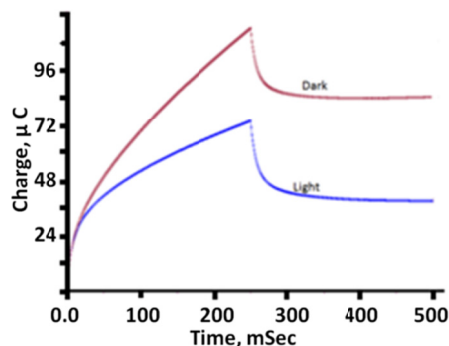
Figure 8. Chronocoulometry of Zn-WO$_3$/ P3ThA in Acetate buffer pH 8. between -0.3 V and -0.7V vs Ag/AgCl A) double layer charge is 15 µC under illumination B) double layer charge is 4.3 µC under dark

3.3 Band-energy Map of P3THA

The data obtained from Figures 3,4 and 5 were used to obtain information about ionization potential (IP) and electron affinity (EA). These important parameters along with the band gap (E_g), are used to draw the energy map of P3THA. These parameters are also needed to explain the electrical and optical properties of the film. The formula used to determine IP, EA, E_{Fermi}, are mentioned elsewhere (Kasem K. et al 2014). By information, a list of photo-electrochemical data for P3ThA and P3ThA/ Zn-doped WO$_3$ were deduced as well as summarized in Table 1 and Diagram 2 . These data suggest that charge injection is mediated at the IOI interface through hole transfer.

Table 1. Photoelectrochemical data for Zn-WO$_3$/P3ThA assembly

Property	P3ThA	Zn-WO$_3$	Zn-WO$_3$ /P3ThA
Band gap, eV	2.25	2.70	
Onset E_{ox}, V vs Ag/AgCl	0.48		
Flat band pot.,E_{fb},V vs SHE	0.2	-0.2	0.00
Ionization Pot., IP, eV	5.28	7.4	
Electron Affinity EA, eV	≈ 2.9	4.40	
Φ Hole barrier, eV	1.6		
φ Electron barrier ,eV	1.4		

3.4 Photoelectrochemical Behavior of Zn-WO$_3$/P3ThA Aqueous Suspensions

The theory of the photolysis of aqueous $[Fe(CN)_6]^{4-}$ has been discussed elsewhere (Kasem K 2012) . In this study , aqueous suspensions of pure Zn-WO$_3$ and surface-modified with P3ThA in 0.2 M phosphate buffer at pH 6 containing 0.010M $[Fe(CN)_6]^{4-}$ were subject to the photolysis process. The potential of the Pt collector electrode was kept constant at 0.000 V vs Ag/AgCl. The results are displayed in Figure 9. Peak A in Figure 9 is the result of total electrochemical reduction of any $[Fe(CN)_6]^{3-}$ that generated from the following photoreaction:

$$[Fe(CN)_6]^{4-} \ + \ h\nu \ \blacktriangleright \ [Fe(CN)_6]^{3-} \tag{1}$$

In presence of Semiconductors nanoparticles (SC), the following photoreduction reaction takes place :

$$[Fe(CN)_6]^{3-} \ + \ h\nu \ + \ SC(e/h) \ \blacktriangleright \ [Fe(CN)_6]^{4-} \tag{2}$$

Reaction 7 takes place concurrently with reaction 1. The mechanism of reaction in equation 7 has been previously discussed (Kasem K 2012). Since the concentration of $[Fe(CN)_6]^{4-}$ is constant, the decrease in electrochemical reduction current reported in Figure 9B is due to photo-reduction of $[Fe(CN)_6]^{3-}$ generated from reaction 1 by the SC nanoparticles. The par-labeled (electrochemical reduction current) in Figure 9 refers to the maximum current supposed to get if the SC material in photo-inactive. The vertical arrows pointing to peaks in Figure 9 B &C are the qualitative indication of the contribution of the Zn-WO$_3$ (Figure 9 trace B) and Zn-WO$_3$/P3ThA (Figure 9 trace C) to the photoreduction of $[Fe(CN)_6]^{3-}$. Photons consumed in this photoreaction can be quantitatively calculated from the integration of the green zone portion in Figure 9 D. The results displayed in figure 9 clearly show that Zn-WO$_3$ modified with P3ThA was more efficient in the process of photoreduction of $[Fe(CN)_6]^{3-}$ than the native Zn-WO$_3$.
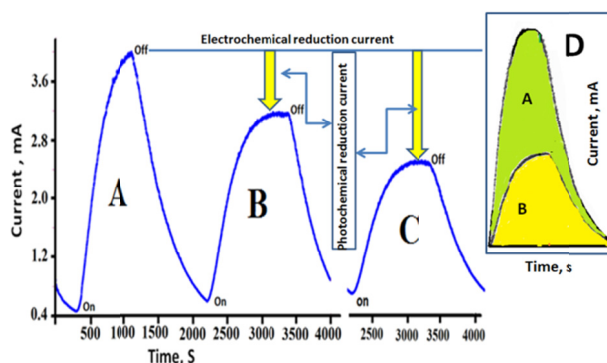
Figure 9. Photolysis in 0.2 M phosphate buffer (pH 6) A) 10 mM of $[Fe(CN)_6]^{4-}$ B) 10 mM of $[Fe(CN)_6]^{4-}$ + Zn-WO$_3$ nanoparticles C) 10 mM of $[Fe(CN)_6]^{4-}$ + Zn-WO$_3$/P3ThA nanoparticles   D) Diagram for electrochemical (yellow) and photochemical current(green)

4. Conclusion

The fact that the Zn-doped WO_3 used in this study is a p-type semiconductor and the properties listed in table 1 for P3THA indicate that the compound is electron acceptor, as evident from it low electron affinity , therefor ,we have created a p-p IOI assembly . This also suggests that an Iso p-p junction [Haibo Wang et al 2010] is formed by creation of hole accumulation layer in one side and hole depletion layer on the counter side. Furthermore, due to the fact that holes in P3THA's HOMO are at a more negative potential than those in Zn-WO_3 's VB (1.6 eV) the charge injection/transfer mechanism took place via hole transfer. This is because the more negative potential will attract Zn-WO_3 holes to P3THA side. We suggest that the mechanism of reduction of $[Fe(CN)_6]^{3-}$ to $[Fe(CN)_6]^{4-}$ took place by (1) retarding the charge recombination process by neutralizing the holes centers first, then (2) electron injection on the adsorbed $[Fe(CN)_6]^{3-}$ as shown the following mechanism :

Step 1 $[Fe(CN)_6]^{4+} + h\nu = [Fe(CN)_6]^{3-} + e_{aq}^-$

Step 2 $[Fe(CN)_6]^{3-}$ + SC nanoparticles ➜ $\{[Fe(CN)_6]^{3-}\}_{ads.}$
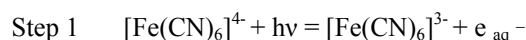
Step 3 $H_2PO_4^-$ acts as a hole scavenger and undergoes photo-oxidation to $H_2PO_4^*$ (Abdullah M. et al, 1990) as follows:

$$SC (e/h) + H_2PO_4^{1-} = H_2PO_4^* + e \text{ (conduction band)}$$

where electrons (e) are in the conduction band, and hole (h) are in the valence band. The hole transfer takes place first to oxidize $H_2PO_4^-$ because of its higher concentration than ferrocyanide anions. Then the hole is neutralized. This suggests that the reduction of ferricyanide follows the hole consumption as shown in step 4:

Step 4 $\{[Fe(CN)_6]^{3-}\}_{ads.}$ + e (from CB) = $\{[Fe(CN)_6]^{4-}\}_{ads.}$
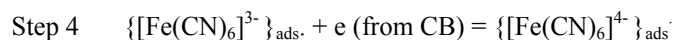
The band-energy map of P3ThA generated a staggered-band alignment with Zn-WO_3 (Figure 10) semiconductors in IOI assemblies as indicated by both electrochemical and spectroscopic data. Such staggered band alignments facilitated the photo-activity of both organic and inorganic semiconductors leading to more capturing of incident photons at this IOI assembly. The assembly Zn-WO_3/P3ThA interface shows better photon capturing than the Zn-WO_3 alone P3ThA captures more photons of incident radiation that match its low band gap.

The fact that more $Fe(CN)_6]^{3-}$ is reduced photochemically by the Zn-WO_3/P3ThA assembly than that with the native Zn-WO_3 only, suggests that this assembly is more efficient in hydrogen production because of its role in making reaction in equation 6 reversible.
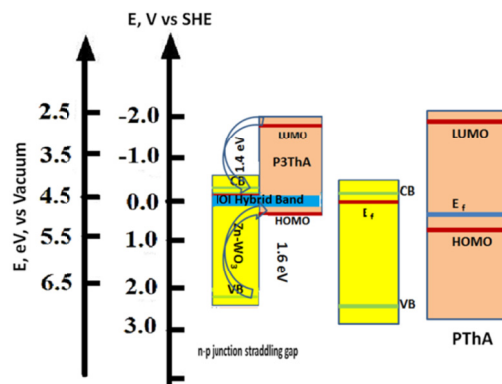
Figure 10. Energy band alignments for the Zn-WO_3/P3ThA assembly

Acknowledgment

References

Abdullah, M., Low, G. K. C., & Matthews, R. W. (1990). Effects of common inorganic anions on rates of photocatalytic oxidation of organic carbon over illuminated titanium dioxide. *J. Phys. Chem., 94*(17), 6820. http://dx.doi.org/10.1021/j100380a051

Bondock, S., Fadaly, W., & Metwally, M. A. (2010). Synthesis and antimicrobial activity of some new thiazole, thiophene and pyrazole derivatives containing benzothiazole moiety. *European Journal of Medicinal Chemistry, 45*(9), 3692-3701. http://dx.doi.org/10.1016/j.ejmech.2010.05.018

Gerald, Z., Antonio, C., Helmut, N., Rafael, G., José, L. S., Nazario, M., … Sariciftci, N. S. (2001).

Photoinduced Charge Carriers in a Donor-Acceptor Double-Cable Polythiophene with Covalently Bound Tetracyanoanthraquinodimethane Moieties. *Mat. Res. Soc. Symp. Proc., 660,* Materials Research Society, JJ8.11.1-6.

Haibo, W., & Donghang, Y. (2010). Organic heterostructures in organic field-effect transistors. *NGP Asia materials, 2*(2), 69. http://dx.doi.org/10.1038/asiamat.2010.44

Kalyanasundaram, & Grätzel, M. (1998). Applications of functionalized transition metal complexes in photonic and optoelectronic devices. *Chem. Rev., 77,* 347. http://dx.doi.org/10.1016/S0010-8545(98)00189-1

Kasem, K., & Davis, C. (2008). Photoelectrochemical studies on colloidal copper (I) oxide/modified with some organic semiconductors: Incentive for use of nanoparticle systems. *Bulletin of Mat Sci., 31*(7), 925. http://dx.doi.org/10.1007/s12034-008-0147-5

Kasem, K., Menges, S., & Jones, S. (2009). Photoelectrochemical studies on poly[1-(2-aminophenyl)pyrrole] — Creation of a photoactive inorganic–organic semiconductor interface (IOI). *Canad. J. Chem., 87*(8), 1109. http://dx.doi.org/10.1139/V09-079

Kasem, K., Bennett, W, Daanen, N., & Dalla, P. G. (2014). Photoelectrochemical Studies at TiO2/Poly 2-Anilino 1,4 Naphthoquinone Interfaces. *J. Surface and interface materials, 2*, 1-7.

Kasem, K. K. (2012). Role of Platinum in Photoelectrochemical Studies Related to Solar Energy Harvesting. *Platinum Metal Review, 56*(4), 221-228. http://dx.doi.org/10.1595/147106712X654178

Kim, J. H., Park, J. B., Shin, S. A., Hyun, M. H., & Hwang, D. H. (2014). Low-bandgap copolymers consisting of 2,1,3-benzoselenadiazole and carbazole derivatives with thiophene or selenophene π-bridges. *Polymer, 55(*16), 3605-3613. http://dx.doi.org/10.1016/j.polymer.2014.05.055

Kumar, P., Ranjith, K., Gupta, S., & Ramamurthy, P. C. (2011). Electrochemical copolymerization of thiophene derivatives; a precursor to photovoltaic devices. *Electrochimica Acta, 56*(24), 8184-8191. http://dx.doi.org/10.1016/j.electacta.2011.06.114

Liao, D. L., Badour, C. A., & Liao, B. Q. (2008). Preparation of nanosized TiO2/ZnO composite catalyst and its photocatalytic activity for degradation of methyl orangeOriginal. *Journal of Photochemistry and Photobiology A: Chem., 194*, 11. http://dx.doi.org/10.1016/j.jphotochem.2007.07.008

Pengchao, S., Chi, Q., Li, Z., Ulstrup, J., Moller, P. J., & Mortensen, J. (2007). Functional Polythiophene Nanoparticles: Size-Controlled Electropolymerization and Ion Selective Response. *Journal of the American Chemical Society, 129*(13), 3888-3896. http://dx.doi.org/10.1021/ja067193w

Thomas, K. G., & Kamat, P. V. (2003). Chromophore-Functionalized Gold Nanoparticles. *Acc. Chem. Res., 36*, 888. http://dx.doi.org/10.1021/ar030030h

Vacareanu, L., Ivan, T., & Grigoras, M. (2012). New symmetrical conjugated thiophene-azomethines containing triphenylamine or carbazole units: Synthesis, thermal and optoelectrochemical properties. *High Performance –Polymers, 24*(8), 717-729. http://dx.doi.org/10.1177/0954008312450595

Wang, C., Zhao, J., Wang, X., Mai, B., Sheng, G., Peng, P., & Fu, J. (2002). Preparation, characterization and photocatalytic activity of nano-sized ZnO/SnO2 coupled photocatalysts. *Appl. Catal., B: Environ., 39*, 269–279. http://dx.doi.org/10.1016/S0926-3373(02)00115-7

Wang, Y., Su, Y. R., Qiao, L., Liu, L. X., Su, Q., Zhu, C. Q., & Liu, X. Q. (2011). Synthesis of one-dimensional TiO2/V2O5 branched heterostructures and their visible light photocatalytic activity towards Rhodamine B. *Nanotechnology, 22,* 225702. http://dx.doi.org/10.1088/0957-4484/22/22/225702

Yu-Ra, J., Lee, S. H., Lee, Y. S., Hwang, Y. H., Pyo, M., & Zong, K. (2011). Synthesis of selenopheno[3,2-c]thiophene derivatives and (opto)electrochemical properties of new low bandgap conjugated polymers. *Synthetic Metals, 161*(13-14), 1444-1447. http://dx.doi.org/10.1016/j.synthmet.2011.04.014

Zhang, Q., Wu, T., Bu, X., Tran, T., & Feng, P. (2008). Ion Pair Charge-Transfer Salts Based on Metal Chalcogenide Clusters and Methyl Viologen Cations. *Chem. of Mate., 20*(13), 4170. http://dx.doi.org/10.1021/cm800904d

Copyrights